Breast Tissue Classification in Digital Breast Tomosynthesis Images using Texture Features: A Feasibility Study

Despina Kontos, Rachelle Berger, Predrag R. Bakic and Andrew D.A. Maidment
University of Pennsylvania, Department of Radiology, 3400 Spruce St., Philadelphia PA 19104
{Despina.Kontos | Rachelle.Berger | Predrag.Bakic| Andrew.Maidment} @uphs.upenn.edu

ABSTRACT

Mammographic breast density is a known breast cancer risk factor. Studies have shown the potential to automate breast density estimation by using computerized texture-based segmentation of the dense tissue in mammograms. Digital breast tomosynthesis (DBT) is a tomographic x-ray breast imaging modality that could allow volumetric breast density estimation. We evaluated the feasibility of distinguishing between dense and fatty breast regions in DBT using computer-extracted texture features. Our long-term hypothesis is that DBT texture analysis can be used to develop 3D dense tissue segmentation algorithms for estimating volumetric breast density. DBT images from 40 women were analyzed. The dense tissue area was delineated within each central source projection (CSP) image using a thresholding technique (*Cumulus*, Univ. Toronto). Two $(2.5cm)^2$ ROIs were manually selected: one within the dense tissue region and another within the fatty region. Corresponding $(2.5cm)^3$ ROIs were placed within the reconstructed DBT images. Texture features, previously used for mammographic dense tissue segmentation, were computed. Receiver operating characteristic (ROC) curve analysis was performed to evaluate feature classification performance. Different texture features appeared to perform best in the 3D reconstructed DBT compared to the 2D CSP images. Fractal dimension was superior in DBT (AUC=0.90), while contrast was best in CSP images (AUC=0.92). We attribute these differences to the effects of tissue superimposition in CSP and the volumetric visualization of the breast tissue in DBT. Our results suggest that novel approaches, different than those conventionally used in projection mammography, need to be investigated in order to develop DBT dense tissue segmentation algorithms for estimating volumetric breast density.

Keywords: Breast, classifier design, digital breast tomosynthesis, dense tissue classification, texture analysis.

1. INTRODUCTION

There is growing evidence to suggest that mammographic breast percent density, estimated as the percentage of dense (*i.e*. fibroglandular) tissue in the breast, is an independent risk factor for breast cancer [1]. To date, no fully-automated and reproducible methods have been validated for accurately quantifying breast density. The most commonly used method relies on a semi-automated image processing algorithm in which the dense tissue region is manually segmented in mammograms using image gray-level thresholding. Mammographic breast density is then estimated as the percent of dense tissue area within the entire breast region [1]. Although widely used for breast cancer risk estimation, these approaches are highly subjective and difficult to standardize, potentially limiting their applicability as breast cancer risk assessment tools for the general population. On the other hand, recent studies [2-4] have shown the potential to automate the segmentation of dense tissue in mammograms using computer-extracted texture features. These studies suggest that computerized texture features could be used to develop fully-automated, objective, and reproducible methods to quantify breast density for breast cancer risk estimation.

Conventional mammography, however, has limitations for performing texture and density analysis. Mammograms are projection x-ray images in which the breast tissue layers are superimposed. As a result, mammographic texture features reflect properties of an admixture of tissues, including dense, fatty, and superficial skin tissue layers. In addition, being a projection imaging technique, mammography does not allow estimation of the true volumetric breast density (*i.e*. the percent volume of dense tissue within the entire breast volume), but rather an estimate of density measured from the projection of overlapping dense tissues [5]. Current research efforts are focusing on developing methods to estimate volumetric breast density from mammographic images by incorporating breast thickness information; alternative 3D imaging modalities such as breast ultrasound and MRI are also being considered [6].

Medical Imaging 2009: Computer-Aided Diagnosis, edited by Nico Karssemeijer, Maryellen L. Giger
Proc. of SPIE Vol. 7260, 726024 · © 2009 SPIE · CCC code: 1605-7422/09/$18 · doi: 10.1117/12.813812

Digital breast tomosynthesis (DBT) is a 3D x-ray breast imaging modality in which tomographic images of the breast are reconstructed from multiple low-dose 2D x-ray source projection images [7]. DBT alleviates the effect of tissue superimposition, offering superior parenchymal texture visualization compared to mammography. Our previous studies have shown preliminary evidence that DBT texture analysis could potentially result in more discriminative features to characterize breast density patterns in comparison to projection mammography [8]. Our long-term hypothesis is that DBT texture analysis could be used to develop fully-automated 3D dense tissue segmentation algorithms to compute volumetric breast density for breast cancer risk estimation.

As a first step towards this goal, we evaluated the feasibility of distinguishing between dense and fatty breast tissue regions in DBT images by using computer-extracted texture features. Both source projections and fully-reconstructed DBT images were analyzed. Various texture descriptors were estimated and their relative classification performance in distinguishing between the dense and fatty breast tissue regions was evaluated.

2. METHODS

2.1. Dataset

Contralateral DBT images from 40 women with recently detected abnormalities and/or previously diagnosed breast cancer were analyzed. The images were retrospectively collected under IRB approval and HIPAA regulations from a multimodality breast imaging clinical trial that has been completed in our department[†]. DBT acquisition was performed with a GE Senographe 2000D FFDM system modified to allow positioning of the x-ray tube at 9 locations by varying the angle from -25^{o} to $+25^{o}$ with increments of 6.25^{o}. The breast was compressed in an MLO position and source projections were acquired with spatial resolution of 0.1mm/pixel. Filtered-backprojection was used to reconstruct DBT tomographic planes in 1mm increments with 0.22mm in-plane resolution.

The dense tissue area was delineated within each central source projection (CSP) by an experienced medical physicist using *Cumulus* (Ver. 4.0, Univ. Toronto), the widely validated software for breast percent density estimation[1]. CSP images are equivalent to a low-dose mammogram visualizing the breast with the same positioning as the corresponding reconstructed DBT image. Two $(2.5\ cm)^2$ ROIs (256x256 pixels at 0.1mm/pixel resolution) were manually selected in the CSP images: one within the region of dense breast tissue and another within the adipose tissue region (Fig. 1). The placement of the ROIs was randomly chosen within the dense and fatty breast tissue region in each CSP image, in order to provide a random sample of the properties of the different tissue types. Corresponding $(2.5cm)^3$ ROIs (116x116 pixels at 0.22mm/pixel resolution) were placed within the fully-reconstructed 3D DBT image using an automated projective coordinate transformation into the x-y plane of the central reconstructed tomographic slice (Fig. 2).

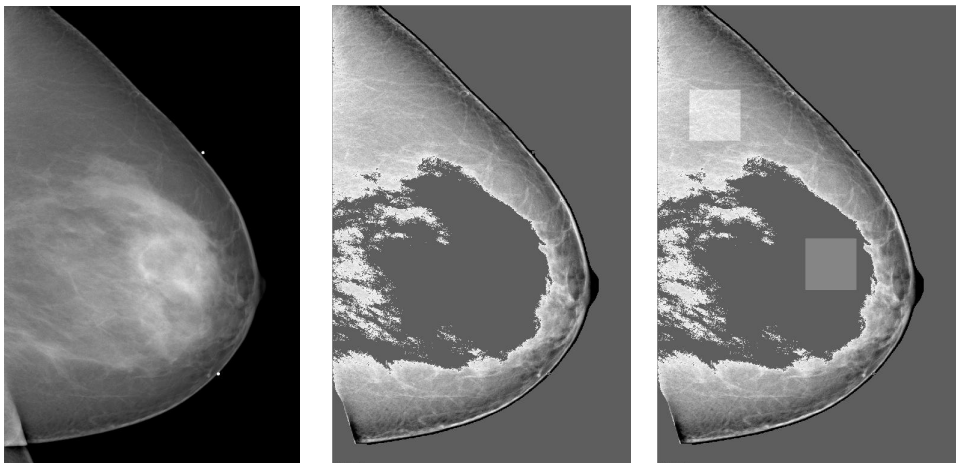

(a) (b) (c)

Fig. 1 Examples of (a) a digital breast tomosynthesis (DBT) central source projection (CSP), with (b) the corresponding dense tissue region segmented within the breast region, and (c) the selected dense and fatty tissue ROIs.

[†] Evaluation of Multimodality Breast Imaging, NIH P01 CA85484, PI: M. Schnall

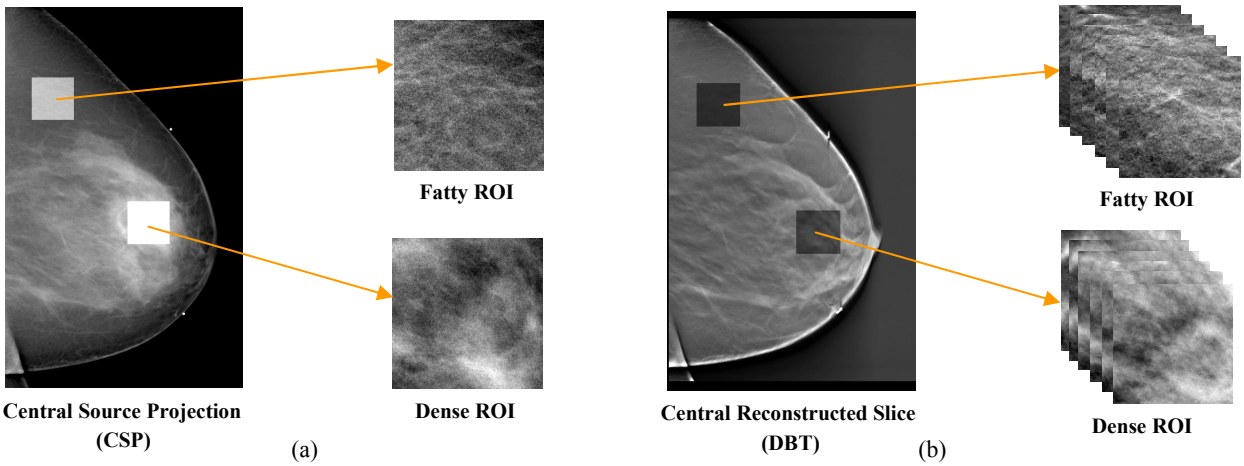

Fig. 2 Examples of dense and fatty ROIs selected in (a) a central source projection (CSP) and (b) the corresponding digital breast tomosynthesis (DBT) ROIs centered within the breast volume by a projective coordinate transformation on to the central DBT plane.

2.2. Texture feature extraction

Texture features of skewness, coarseness, contrast, energy, homogeneity and fractal dimension were computed from both the 2D CSP and the 3D DBT ROIs using our previously developed texture analysis techniques [8]. These features have been shown to have value in segmenting the dense tissue region in previous studies with mammograms [4]. We have also recently shown that these texture features tend to correlate to breast density when computed from DBT images [8].

Two approaches were implemented for texture analysis in the 3D reconstructed DBT images: (i) tomographic and (ii) volumetric texture analysis. For each imaging modality, the individual texture features were also combined into one representative feature using principal component analysis (PCA) [9].

2.2.1. Tomographic (2D) texture analysis

For each texture descriptor, a feature f_i, i=1,…,T was computed from each tomographic slice of the 3D DBT ROI (T=26 slices in each ROI, 1mm/slice), resulting in a feature vector $F_T = [f_1,\ldots,f_T]$ for each ROI. The mean of the feature vector, $\overline{F_T}$, was used as the representative feature for the ROI.

Skewness is the third statistical moment and was computed as:

$$skewness = \frac{w_3}{w_2^{3/2}} \quad , \quad w_k = \sum_{i=0}^{g_{max}} n_i \left(i - \bar{i}\right)^k \Big/ N \quad , \quad N = \sum_{i=0}^{g_{max}} n_i \quad , \text{ and } \quad \bar{i} = \sum_{i=0}^{g_{max}} \left(i n_i / N\right) \qquad \textbf{(Eq. 1)}$$

where n_i represents the number of times that gray level value i occurs in the image region, g_{max} is the maximum gray-level value, and N is the total number of image pixels.

The computation of coarseness is based on the neighborhood grey-tone difference matrix (NGTDM) [10, 11] of the gray-level values within the image region; this matrix is derived by calculating the difference between the gray-level value of each pixel and the average gray-level value of the pixels around a neighborhood window.

$$coarseness = \left(\sum_{i=0}^{g_{max}} p_i v(i)\right)^{-1} \quad , \text{ and } \quad v(i) = \begin{Bmatrix} \sum \left|i - \overline{L_i}\right| \; for \; i \in \{n_i\} \; if \; n_i \neq 0 \\ 0 \quad otherwise \end{Bmatrix} \qquad \textbf{(Eq. 2)}$$

where $v(i)$ is the NGTDM. In the above formulas, g_{max} is the maximum gray-level value, p_i is the probability that gray level i occurs, $\{n_i\}$ is the set of pixels having gray level value equal to i, and $\overline{L_i}$ is given by:

$$\overline{L_i} = \frac{1}{S-1} \sum_{k=-t}^{t} \sum_{l=-t}^{t} j(x+k, y+l) \qquad \textbf{(Eq. 3)}$$

where $j(x,y)$ is the pixel located at (x,y) with gray level value i, $(k,l)\neq(0,0)$ and $S=(2t+1)^2$ with t=1 specifying the neighborhood size around the pixel located at (x,y).

Contrast, energy, and homogeneity, as proposed originally by Haralick [12], require the computation of second-order statistics derived from the gray-level co-occurrence matrix; the spatial dependence of gray-levels is estimated by calculating the frequency of the spatial co-occurrence of gray-levels in the image [12].

$$\text{contrast} = \sum_{i=0}^{g_{\max}} \sum_{j=0}^{g_{\max}} |i-j|^2 C(i,j) \quad , \quad \text{energy} = \sum_{i=0}^{g_{\max}} \sum_{j=0}^{g_{\max}} C(i,j)^2 \quad , \quad \text{homogeneity} = \sum_{i=0}^{g_{\max}} \sum_{j=0}^{g_{\max}} \frac{C(i,j)}{1+|i-j|} \qquad \textbf{(Eq. 4)}$$

where g_{max} is the maximum gray-level value and C is the normalized co-occurrence matrix [12]. To optimize the computation of the gray-level co-occurrence statistics, gray-level quantization was implemented [13]. The co-occurrence frequencies were calculated symmetrically in the four directions around each pixel using a displacement of one pixel offset along x and y dimensions. The texture features calculated in each of these four directions were averaged to create a single measure that was used in our experiments.

Fractal dimension (FD) was estimated based on the power spectrum of the Fourier transform of the image [14, 15]. The 2D Discrete Fourier Transform (DFT) was performed using the Fast Fourier Transform (FFT) algorithm

$$F(u,v) = \sum_{m=0}^{M-1} \sum_{n=0}^{N-1} I(m,n) e^{-j(2\pi/\mathrm{M})um} e^{-j(2\pi/N)vn}, \quad u = 0,1,...,M-1 \quad v = 0,1,...N-1 \qquad \textbf{(Eq. 5)}$$

where I is the 2D image region of size (M, N), and u and v are the spatial frequencies in the x and y directions. The power spectral density P was estimated from $F(u,v)$ as

$$P(u,v) = |F(u,v)|^2 \qquad \textbf{(Eq. 6)}$$

To compute the FD, P was averaged over radial slices spanning the FFT frequency domain. The frequency space was uniformly divided in 24 directions, with each direction uniformly sampled at 30 points along the radial component. To calculate the FD the least-squares-fit of the $log(P_f)$ versus $log(f)$ was estimated, where $f = \sqrt{u^2+v^2}$ denotes the radial frequency [14]. The FD is related to the slope β of this log-log plot by:

$$FD = \frac{3D_T + 2 - \beta}{2} \qquad \textbf{(Eq. 7)}$$

where D_T is the topological dimension. For a 2D image D_T=2 and $FD = (8 - \beta)/2$.

2.2.2. Volumetric (3D) texture analysis

The conventional 2D texture descriptors were extended to 3D by considering a 3D neighborhood of voxels (*i.e.* volume elements), rather than a 2D neighborhood of pixels, when computing gray-level texture statistics.

Skewness was again computed as the third moment of the gray-level histogram as in **Eq 1**; however, the gray-level histogram of the ROI was estimated using the gray-level values from the entire 3D ROI volume, rather than separately for each tomographic plane. This is valid since skewness does not depend on the spatial co-occurrence of gray-levels.

For coarseness, the local differences in gray-level values, required for the computation of the NGTDM, were estimated within a 3D neighborhood of voxels. More specifically the definition of $\overline{L_i}$ in **Eq. 3** was modified, to account for a 3D rather than a 2D neighborhood of voxels as follows:

$$\overline{L_i} = \frac{1}{S-1} \sum_{k=-t}^{t} \sum_{l=-t}^{t} \sum_{q=-t}^{t} j(x+k, y+l, z+q) \qquad \textbf{(Eq. 8)}$$

Here $j(x,y,z)$ is the voxel located at (x,y,z) with gray level value i, $(k,l,z) \neq (0,0,0)$, and $S=(2t+1)^3$ with $t=1$ specifying the 3D voxel window around (x,y,z).

For contrast, energy, and homogeneity, the gray-level co-occurrence statistics, required for the computation of the co-occurrence matrix in **Eq. 4**, were estimated based on the spatial co-occurrence frequencies of voxel gray-level values within the entire 3D ROI volume similar to the approach of Chen *et al.* [16]. A 3D displacement of one voxel offset was defined along the x, y, and z dimensions resulting in 26 neighboring voxel-pairs in 13 independent symmetric directions. Texture features were calculated in each of these 13 directions and they were averaged to create a single measure that was used in our experiments.

Fractal dimension (FD) was estimated based on the power spectrum of the 3D Fourier transform of the image. The 3D DFT was performed for the entire 3D ROI using the FFT algorithm:

$$F(u,v,w)=\sum_{m=0}^{M-1}\sum_{n=0}^{N-1}\sum_{k=0}^{K-1} I(m,n,k)e^{-j(2\pi/\mathrm{M})um}e^{-j(2\pi/N)vn}e^{-j(2\pi/K)wk} \quad \textbf{(Eq. 9)}$$

where I is the 3D image region of size (M, N, K), and u, v and w are the spatial frequencies in the x, y, and z directions respectively. The power spectral density (PSD) was estimated as:

$$P(u,v,w)=|F(u,v,w)|^2 \quad \textbf{(Eq. 10)}$$

To compute the FD, P was averaged over radial sectors spanning the 3D FFT frequency domain. The frequency space was evenly divided in 24 azimuth and 12 zenith directions, and each direction was uniformly sampled at 30 points along the radial component. To calculate the FD, the least-squares-fit of the $log(P_f)$ versus $log(f)$ was estimated, where $f=\sqrt{u^2+v^2+w^2}$ denotes the radial frequency in spherical coordinates [14]. The FD is related to the slope β of this log-log plot as defined in **Eq. 7;** for D_T=3 in 3D, $FD = (11-\beta)/2$.

3.1. Data analysis

Two-tailed paired Student's t-test was applied to estimate the difference in the means of the texture feature distributions between the dense and the fatty ROIs for each imaging modality. Associated p-values were estimated to assess statistical significance. Receiver operating characteristic (ROC) curve analysis was performed using the proper binormal model of the DBM MRMC software (Ver. 2.2 by the Univ. of Chicago and Univ. of Iowa)[17-20] to evaluate the performance of the texture features in distinguishing between the dense and fatty ROIs. ROC area under the curve (AUC) was compared across the different imaging modalities and the different feature extraction techniques.

3. RESULTS

The Student's t-test analysis shows that most of the estimated texture features are statistically significantly different between the dense and the fatty ROIs both in the CSP and the DBT images (Table 1). However, different texture features are more discriminative between breast tissue types for the two imaging modalities. Coarseness, contrast and homogeneity are more discriminative in the CSP ROIs ($p<0.001$), while energy and fractal dimension are more discriminative in the DBT ROIs ($p<0.001$). The volumetric texture features are generally more discriminative than the tomographic texture features for the DBT ROIs, as demonstrated both by the PCA and the individual texture features (Table 1). Representative box-plots are shown in Figure 3 for contrast, fractal dimension and the PCA texture feature.

Table 1. *P*-values from applying two-tailed paired Student's t-test to compare the means of the texture feature distributions between the dense and the fatty ROIs in central source projection (CSP) images, and in digital breast tomosynthesis (DBT) images using tomographic (DBT 2D) and volumetric (DBT 3D) texture analysis (* for $p\leq0.01$, ** for $p\leq0.001$).

T-test *p*-values for dense vs. fatty ROI texture differences			
Texture Features	**CSP**	**DBT 2D**	**DBT 3D**
Skewness	0.50	0.02	0.02
Coarseness	<0.001 **	0.17	0.03
Contrast	<0.001 **	0.78	0.93
Energy	0.001 **	<0.001 **	<0.001 **
Homogeneity	<0.001 **	0.03	0.04
Fractal Dimension	0.19	0.002 *	<0.001 **
PCA Feature	<0.001 **	0.008	<0.001 **

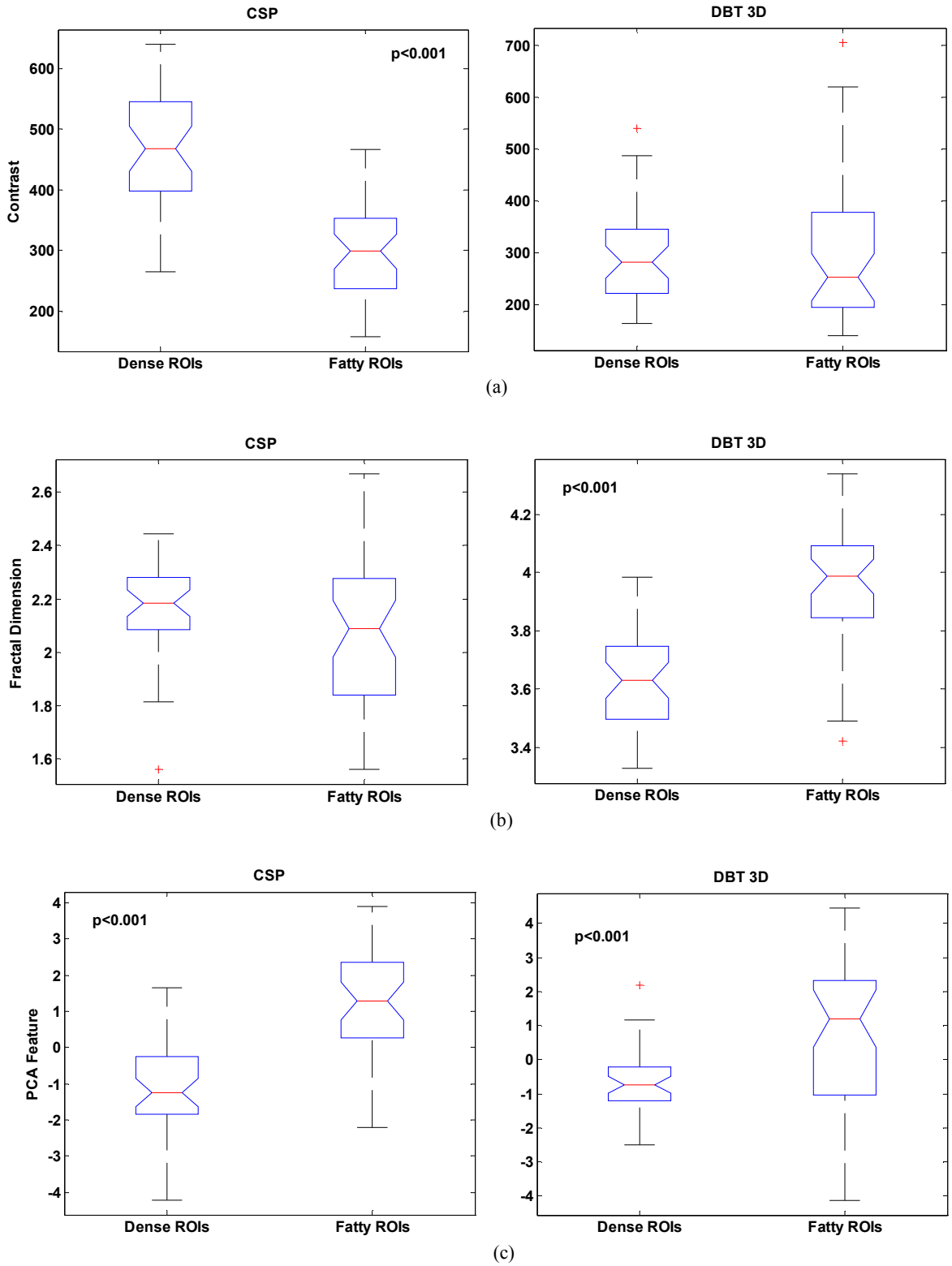

Fig. 3 Box-plots for the most discriminative features (a) contrast in central source projections (CSP) and (b) fractal dimension in digital breast tomosynthesis using volumetric texture analysis (DBT 3D), and (c) the principal component analysis (PCA) feature.

The ROC curve analysis also demonstrates that different features better distinguish between the dense and fatty breast tissue types in the projection CSP images compared to the reconstructed DBT images (Table 2). Contrast and homogeneity have the best classification accuracy in the CSP images (AUC_Z=0.92 and AUC_Z=0.90), while fractal dimension has the best performance in the DBT images (AUC_Z=0.90). Overall, the volumetric texture features perform better in comparison to their tomographic counterparts for the DBT images (PCA AUC_Z=0.78 vs. AUC_Z=0.74). Figure 4 shows comparative ROC curves and the associated AUC estimates for contrast and fractal dimension. Figure 5 shows the corresponding ROC curves for the PCA texture feature.

Table 2. Receiver operating characteristic (ROC) area under the curve (AUC) for distinguishing between dense and fatty breast tissue regions in central source projections (CSP) and fully reconstructed digital breast tomosynthesis (DBT) images using tomographic (DBT 2D) and volumetric (DBT 3D) texture analysis.

AUC (A_z)			
Texture Features	**CSP**	**DBT 2D**	**DBT 3D**
Skewness	0.54	0.66	0.68
Coarseness	0.79	0.74	0.79
Contrast	0.92	0.61	0.58
Energy	0.78	0.76	0.75
Homogeneity	0.90	0.63	0.63
Fractal Dimension	0.62	0.76	0.90
PCA Feature	0.85	0.74	0.78

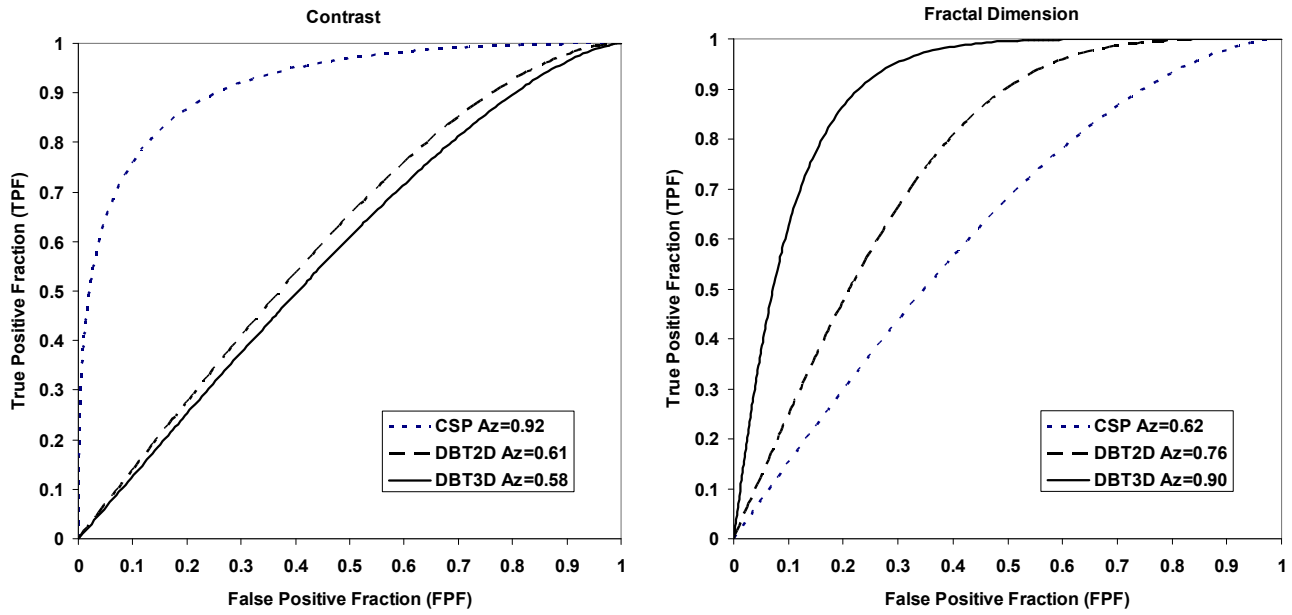

(a) (b)

Fig. 4 Receiver operating characteristic (ROC) curves with associated area under the curve (AUC) for the best performing features (a) contrast and (b) fractal dimension for the central source projection (CSP) ROIs and the fully reconstructed digital breast tomosynthesis (DBT) ROIs using tomographic (DBT 2D) and volumetric (DBT 3D) texture analysis .

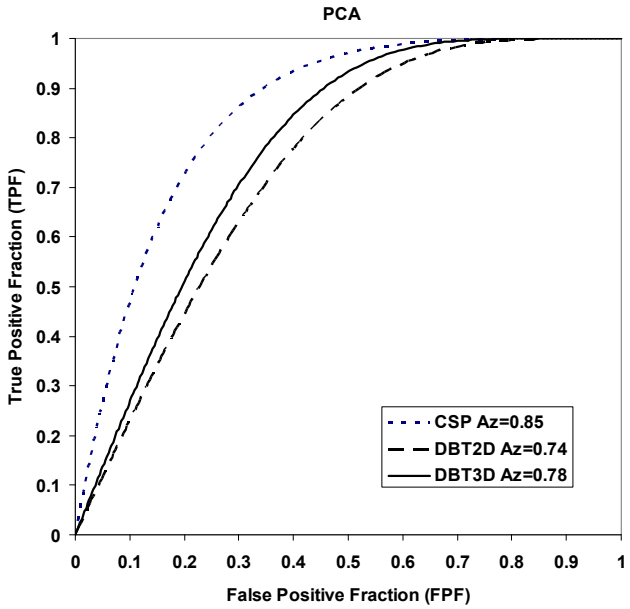

Fig. 5 Receiver operating characteristic (ROC) curves with associated area under the curve (AUC) for the PCA texture feature for the central source projection (CSP) ROIs and the fully reconstructed digital breast tomosynthesis (DBT) ROIs using tomographic (DBT 2D) and volumetric (DBT 3D) texture analysis .

4. DISCUSSION

We attribute the observed differences in feature classification performance to the corresponding differences in parenchymal tissue visualization between the CSP and the DBT images. Due to the projective nature of the CSP image acquisition, the corresponding gray-level pixel values in the CSP image reflect properties of x-ray attenuation throughout the entire thickness of the compressed breast volume. Therefore, texture features such as contrast and homogeneity that depend on the pixel-wise additive effect of superimposed breast tissue types are enhanced. On the other hand, due to the tomographic separation of the breast tissue layers in DBT, the dominant contribution to the gray-level values in the DBT images is the x-ray attenuation at the specific voxel in the breast volume. Therefore, volumetric parenchymal properties such as self-similarity reflected by fractal dimension could be more accurately estimated by the corresponding DBT texture features. Figure 6 shows an illustrative example of this effect in a CSP image in comparison to the central reconstructed slice of the corresponding DBT image. DBT texture analysis could be more advantageous in capturing volumetric parenchymal properties and potentially provide the basis to estimate volumetric breast density in the future.

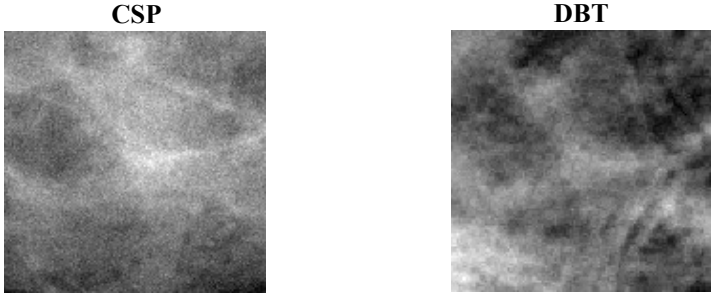

(a) (b)

Fig. 6 An example of corresponding dense tissue regions in (a) the CSP image where dense tissue layers are superimposed and (b) the central reconstructed plane of the digital breast tomosynthesis image (DBT) where the effect of tissue superposition is alleviated.

5. CONCLUSION

Parenchymal texture differs between dense and fatty breast tissue regions both in 2D CSP and fully-reconstructed 3D DBT images. However, different texture features appear to perform best in DBT, in comparison to CSP images. Our results suggest that novel approaches, potentially different than those conventionally used in projection mammography, need to be investigated in order to develop DBT dense tissue segmentation algorithms for estimating volumetric breast density. Further work is underway to determine the optimal texture feature extraction techniques in DBT, investigate the effect of the reconstruction algorithm, and compare to digital mammography.

ACKNOWLEDGEMENT

This work was funded by the Siemens/ Radiological Society of North America (RSNA) Research Fellow Grant (RF0707), by the Susan G. Komen for the Cure Foundation Postdoctoral Fellowship (KG080756), and by the National Institutes of Health/National Cancer Institute Program Project Grant P01-CA85484. We would also like to thank Dr. Ann-Katherine Carton for facilitating image acquisition and Dr. Johnny Kuo for developing and maintaining the RSNA Medical Imaging Resource Center (MIRC) image archive.

REFERENCES

[1] Boyd, N.F., Guo, H., Martin, L.J, et al., "Mammographic density and the risk and detection of breast cancer," New England Journal of Medicine 356(3), 227-236 (2007).
[2] Karssemeijer, N., "Automated classification of parenchymal patterns in mammograms," Physics in Medicine & Biology 43(2), 365-378 (1998).
[3] Zhou, C., Chan, H.P., Petrick, N., et al., "Computerized image analysis: estimation of breast density on mammograms," Medical Physics 28(6), 1056-1069 (2001).
[4] Oliver, A., Freixenet, J., Mart, R., et al., "A novel breast tissue density classification methodology," IEEE Transactions on Information Technology in Biomedicine 12(1), 55-65 (2008).
[5] Kopans, D.B., "Basic physics and doubts about relationship between mammographically determined tissue density and breast cancer risk," Radiology 246(2), 348-353 (2008).
[6] Yaffe, M.J., "Mammographic density. Measurement of mammographic density," Breast Cancer Research 10(3), 209-219 (2008).
[7] Park, J.M., Franken, E.A., Jr., Garg, M., Fajardo, L.L., Niklason, L.T., "Breast tomosynthesis: present considerations and future applications," Radiographics 27(Suppl 1), S231-240 (2007).
[8] Kontos, D., Bakic, P.R., Troxel, A.B., Conant, E.F., Maidment, A.D.A., "Digital breast tomosynthesis parenchymal texture analysis for breast cancer risk estimation: A preliminary study," In: E. A. Krupinski (ed.), Digital Mammography (IWDM), Springer Lectures Notes in Computer Science (LNCS) 5116, 491-498 (2008).
[9] Duda, R., Hart, P., Stork, D., Pattern Classification, John Wiley and Sons (2000).
[10] Li, H., Giger, M.L., Olopade, O.I., Margolis, A., Lan, L., Chinander, M.R., "Computerized Texture Analysis of Mammographic Parenchymal Patterns of Digitized Mammograms," Academic Radiology 12, 863-873 (2005).
[11] Amadasum, M., King, R., "Textural features corresponding to textural properties," IEEE Transactions on Systems Man and Cybernetics 19, 1264–1274 (1989).
[12] Haralick, R.M., Shanmugam, K., Dinstein, I., "Textural features for image classification," IEEE Transactions on Systems, Man and Cybernetics 3, 610–621 (1973).
[13] Kontos, D., Bakic, P.R., Maidment, A.D.A., "Texture in digital breast tomosynthesis: A comparison between mammographic and tomographic characterization of parenchymal properties," In Proc. of SPIE Medical Imaging: Computer Aided Diagnosis (6915), San Diego, CA (2008).
[14] Russ, J.C., Fractal Surfaces, New York Plenum Press (1994).
[15] Li, H., Giger, M.L., Olopade, O.I., Chinander, M.R., "Power Spectral Analysis of Mammographic Parenchymal Patterns for Breast Cancer Risk Assessment," Journal of Digital Imaging 21(2), 145-152 (2008).
[16] Chen, W., Giger, M.L., Li, H., Bick, U., Newstead, G.M., "Volumetric texture analysis of breast lesions on contrast-enhanced magnetic resonance images," Magnetic Resonance in Medicine 58(3), 562-571 (2007).
[17] Kurt Rossmann Laboratories for Radiologic Image Research (http://xray.bsd.uchicago.edu/krl/).
[18] Medical Image Perception Laboratory (http://perception.radiology.uiowa.edu).

[19] Pesce, L.L., Metz, C.E., "Reliable and computationally efficient maximum-likelihood estimation of "proper" binormal ROC curves," Academic Radiology 14(7), 814-829 (2007).
[20] Metz, C.E., Pan, X., " "Proper" Binormal ROC Curves: Theory and Maximum-Likelihood Estimation," Journal of Mathematical Psychology 43(1), 1-33 (1999).